ACS APPLIED MATERIALS & INTERFACES

Research Article

www.acsami.org

# Synthesis and Characterization of Green Zn–Ag–In–S and Red Zn–Cu–In–S Quantum Dots for Ultrahigh Color Quality of Down-Converted White LEDs

Hee Chang Yoon, Ji Hye Oh, Minji Ko, Heeyeon Yoo, and Young Rag Do*

Department of Chemistry, Kookmin University, Seoul 136-702, Republic of Korea

**ABSTRACT:** Eco-friendly green Zn–Ag–In–S (ZAIS) and red Zn–Cu–In–S (ZCIS) core/shell-like alloyed quantum dots (QDs) have been synthesized by a facile hot-injection method with a multiple injection approach. Broad full-width at half-maximum (fwhm) of the photoluminescence (PL) emission and tunability of the green ZAIS and red ZCIS QDs were obtained by adopting a low-temperature core growth and high-temperature multiple alloyed reaction. The alloyed green ZAIS and red ZCIS QDs reached PL quantum yields as high as 0.61 and 0.53; fwhm of the PL peaks were as wide as 81 and 106 nm, respectively. This demonstrates the practical realization of white down-converted light-emitting diodes (DC-LEDs), fully covering the whole visible wavelength range and the cyan gap, using two broad fwhm green ZAIS and red ZCIS QDs. We also characterized the vision and color performance using luminous efficacy (LE), color rendering index (CRI), special CRI for strong red ($R_9$), and color quality scale (CQS) of white DC-LEDs incorporated with green ZAIS and red ZCIS QDs at the correlated color temperature (CCT) range of 2700–10 000 K. The tricolor white DC-LED using broad fwhm green-emitting ZAIS and red-emitting ZCIS core/shell-like alloyed QDs exhibits a moderate LE (31.2 lm/W) and ultrahigh color qualities (CRI = 97, $R_9$ = 97, and CQS = 94) with warm white at a CCT of 3500 K.

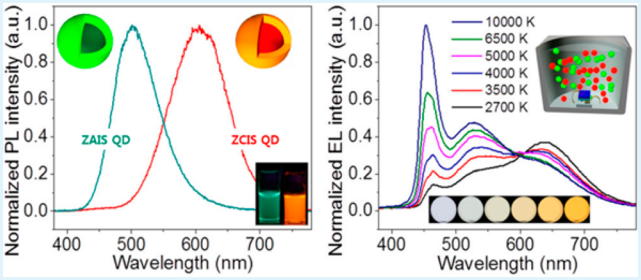


**KEYWORDS:** *quantum dot, AgInS, CuInS, nanophosphor, LED, high-color quality LED*

## INTRODUCTION

Over the past decade, both eco-friendly III–V and I–III–VI based semiconductor quantum dots (QDs) have been intensively investigated in an effort to replace commonly available II–VI based QDs, which are environmentally harmful, which, in turn, limits their suitability for most optoelectronic device applications.[1−7] Various synthetic approaches for highly efficient III–V and I–III–VI based QDs have been studied extensively for application to a variety of unique devices, such as QD-based light-emitting diodes (LEDs),[8,9] white down-converted (DC) LEDs,[10,11] photovoltaic cells,[12,13] and bionanodevices related to biotagging[14,15] due to their excellent optical and electrical properties.

Among the many physical properties of QDs, the full-width at half-maximum (fwhm) of the emission spectrum is one of the key factors to determine the suitability of certain optical properties of QD-based LEDs for applications in QD-LED displays or white DC-LED lighting. As previously reported, it is well-known that III–V type QDs have a narrow emission spectrum; however, I–III–VI type QDs have a broad emission spectrum if the size distribution of QDs is narrowed.[16,17] It is also known that the narrow emission spectrum is mainly due to band-to-band recombination; however, a broad emission spectrum is usually obtained from donor–acceptor (D–A) pair recombination of QDs.[18,19] In view of application to indoor lighting, QDs with a broad spectrum are better for use in the DC layer of white LEDs. The enlarged fwhm of the QD emission spectrum with a homogeneous size distribution makes it possible to improve the color rendering index (CRI) and color quality scale (CQS), which determine the color quality of white light. CRI and CQS are the most important figures of merit of artificial lighting for the evaluation of color performance,[20,21] which compares the spectral power distribution (SPD) of artificial lighting with that from the Sun. Both CRI and CQS of 100 represent ideal white sources.

Before recent developments of I–III–VI based QDs with a broad emission spectrum, most QD-based white DC-LEDs were fabricated by mixing and coating one or two inorganic phosphors and/or one or two narrow-band CdSe-based II–VI[22−27] or InP-based III–V[10,28,29] QDs onto a blue LED to attain a high CRI with warm white. However, CdSe or InP QD-based DC-LEDs have exhibited CRIs of less than 92 with warm white.[27,28] Nonetheless, they are still lower than the best high CRIs of inorganic phosphor-based DC-LEDs.[30,31] Following the development of broad band I–III–VI based QDs for white DC-LEDs,[32−34] $CuInS_2$ based QDs were suggested as a promising red emissive phosphor for warm white LEDs applications.[35] Many approaches using I–III–VI-based QDs

**Received:** January 22, 2015
**Accepted:** March 17, 2015
**Published:** March 17, 2015





DOI: 10.1021/acsami.5b00664
*ACS Appl. Mater. Interfaces* 2015, 7, 7342–7350

Table 1. Properties of I−III−VI QD-based White DC-LEDs in Previously Reported Works

| color-converting materials | luminous efficacy (lm/W) | applied current (mA) | CCT (K) | CRI | ref |
|---|---|---|---|---|---|
| green InP/ZnS + red CIS/ZnS | 45.5 | 20 | 3803 | 90 | 10 |
| yellow YAG:Ce + red CuInS NCs | 91.4 | 20 | 5420 | 81.9 | 35 |
| yellow YAG:Ce + orange | 45.4 | 20 | 4764 | 93.1 | |
| Silicate:Eu + red CuInS QDs | 45.1 | 20 | 3800 | 91.8 | |
| yellow YAG:Ce nanophosphor + red CIS/ZnS QD | 21.1 | 1200 | 3934 | 84.6 | 36 |
| green CIS/ZnS QDs + red CIS/ZnS QDs | 67.8 | 20 | 4694 | 95.3 | 37 |
| | 69.4 | 20 | 5322 | 95.1 | |
| bicolor green and orange CIS/ZnS:Mn/ZnS QD | 61 | 20 | 4000−6000 | 83 | 38 |
| green $Ba_2SiO_4$:Eu + orange CIS/ZnS QD + red CIS/ZnS QD | 32.7 | 20 | 6552 | 90 | 39 |
| green Carbon dots + red Zn−Cu−In−S QDs | | 20 | 5749 | 93 | 40 |
| green CIGS/CIGS-ZnS/ZnS QDs + red InP/ZnS QDs | 34.7 | 20−80 | 5322 | 94 | 41 |
| | | | 3691 | 92 | |

were developed to enhance the CRI of white DC-LEDs and they are summarized in Table 1.[10,35−41] These high CRIs are possible mainly because the emission bandwidths of the I−III−$VI_2$/ZnS QDs available to date are substantially broader, that is, less color-pure to cover the low emission efficiency in the yellow and red regions, than those of their II−VI and III−V rivals. The best reported CRIs of QD-based DC-LEDs were obtained by integrating green and red $CuInS_2$-based QDs with blue emitting InGaN chips. The as-fabricated white DC-LEDs showed a CRI of 95, luminous efficiency of 67.8 lm/W, and correlated color temperature (CCT) of 4694 K.[37] However, the CRI values of green and red I−III−VI-based QD-coated LEDs were still limited to values as high as ∼95 at CCT of ∼4700 K, which is higher than that (2700−3500 K) of warm white. Due to the presence of the cyan gap between the blue LED spectrum and the green QD spectrum in most warm white QD-based DC-LED lighting, a satisfactory solution to produce a green and red QD-based DC-LED (tricolor) structure that can guarantee a high CRI over 95 for use in warm white (CCT of 2700−3500 K) has yet to be reported.

To enhance the CRIs and CQSs of QD-based DC-LEDs at warm white color, it is also necessary to develop broad-band green QDs that can cover the cyan color and have sufficient photoluminescence quantum yield (PL QY). Quite recently, we developed a Zn−Ag−In−S (ZAIS) core/shell-like alloy QD as a member of the solid solution I−III−VI and II−VI QDs, which show a good PL QY (>0.50) with a broad full width at half-maximum (fwhm >85 nm).[32] Compared to the case of typical Zn−Cu−In−S (ZCIS)-based QDs, with the ZAIS-based QDs it is slightly easier to produce bluish green emissive samples with good PL QYs and broad fwhm through the formation of a core/shell-like alloy. In this study, broad fwhm green- and red-emitting non-Cd QDs of ZAIS and ZCIS core/shell-like alloy QDs[42] were synthesized using a facile hot-injection method with multiple injection reactions. The low-temperature core growth and high-temperature alloyed reaction approaches were used to synthesize the core/shell-like alloyed green ZAIS and red ZCIS QDs with broad fwhm of the photoluminescence (PL) emissions. In addition, the emitting wavelengths of the ZAIS QD and ZCIS QD were optimized using a green and red color converter to attain tricolor DC white LEDs with high CRIs and CQSs of over 90 in a wide CCT range from 2700 to 10000 K. Finally, we reported the detailed optical properties of a tricolor white DC-LED with wide fwhm of green ZAIS (>80 nm) and red ZCIS (>100 nm) based QDs that, when combined with a blue LED, can simultaneously achieve CRI > 94, special CRI for strong red ($R_9$) > 79, and CQS > 92 at a wide CCT range between 2700 and 10000 K.

## EXPERIMENTAL METHODS

**Materials.** All chemicals were used without further purification. Silver nitrate ($AgNO_3$, 99%, Aldrich), copper iodide (CuI, 99.999%, Aldrich), indium(III) acetylacetonate ($In(acac)_3$, 99.99%, Aldrich), indium(III) acetate ($In(ac)_3$, 99.99%, Aldrich), sulfur (S, 99.98%, Aldrich), zinc stearate (10−12% Zn basis, Aldrich), zinc acetate dihydrate ($Zn(ac)_2$, reagent grade, Aldrich), 1-octadecene (ODE, 90%, Aldrich), oleic acid (OA, 90%, Aldrich), 1-dodecanethiol (DDT, 98%, Aldrich), oleylamine (OLA, 70%, Aldrich), and trioctylphosphine (TOP, 90%, Aldrich) were obtained from Sigma-Aldrich in order to synthesize ZAIS and ZCIS QDs. Silicone binder (OE-6636 A/B kit, Dow Corning Co.) was obtained to make ZAIS and ZCIS QDs mixed paste. The cup-type InGaN LED ($\lambda_{max}$ = 445 nm, Dongbu LED, Inc.) were utilized as blue light source.

**Synthesis of Green ZAIS QDs.**[32] For AIS core QD growth, 0.1 mmol of $AgNO_3$, 0.4 mmol of $In(acac)_3$, 1.5 mmol of OA, and 25 mmol of ODE were placed into a three-neck flask. The reaction solution was purged through $N_2$ gas for 20 min at room temperature and quickly heated to 90 °C so that 4.0 mmol of DDT could be added as the main capping material into the reaction mixture. After the addition of DDT, the mixture was maintained at the same temperature to allow reaction between the core precursor and DDT for 30 min with $N_2$ gas purging. Then, as the S source of AIS core QDs, 0.65 mmol of S dissolved in 4.0 mmol of OLA was injected into the three-neck flask at 120 °C, and the crude AIS core QD solution was reacted for 3 min. The first shell solution, consisting of 0.4 mmol of Zn stearate and 0.4 mmol of S dissolved in 0.4 mmol of TOP, was then quickly added to the AIS core QD solution. The ZnS shell growth temperature was controlled up to 180 °C, and the reaction pot was maintained at the same temperature to allow the growth of ZAIS for 2 h. After the reaction, the second ZnS shell solution was injected again into the mixture and heated to the reaction temperatures of 210, 220, and 230 °C for 2 h. To control the emission wavelength of the green ZAIS core/shell-like alloy QDs, the third ZnS shell solution was injected again at each reaction temperature and reacted for 2 h. The crude green ZAIS QD solution was purified with centrifugation and stored in chloroform.

**Synthesis of Red ZCIS QDs.**[33] For CIS core QD growth, 0.125 mmol of CuI, 0.5 mmol of $In(ac)_3$, 2 mmol of DDT, and 15 mmol of OLA were placed in a three-neck flask. The reaction solution was degassed for 15 min at 120 °C and purged through $N_2$ gas for 15 min. Subsequently, as the S source of CIS core QD, 3 mmol of S dissolved in 9 mmol of ODE was injected into the three-neck flask at 160 °C, and the crude CIS core QD solution was reacted for 3 min. The first ZnS shell stock solution, consisting of 5.3 mmol of zinc acetate dihydrate dissolved in 16.8 mmol of OA and 8.3 mmol of ODE, was then added drop-wise at a rate of 2.0 mL/min into the CIS core solution, and the reaction temperature was controlled up to 220, 230, and 240 °C for 30 min. After the first ZCIS reaction, the second ZnS


DOI: 10.1021/acsami.5b00664
ACS Appl. Mater. Interfaces 2015, 7, 7342−7350

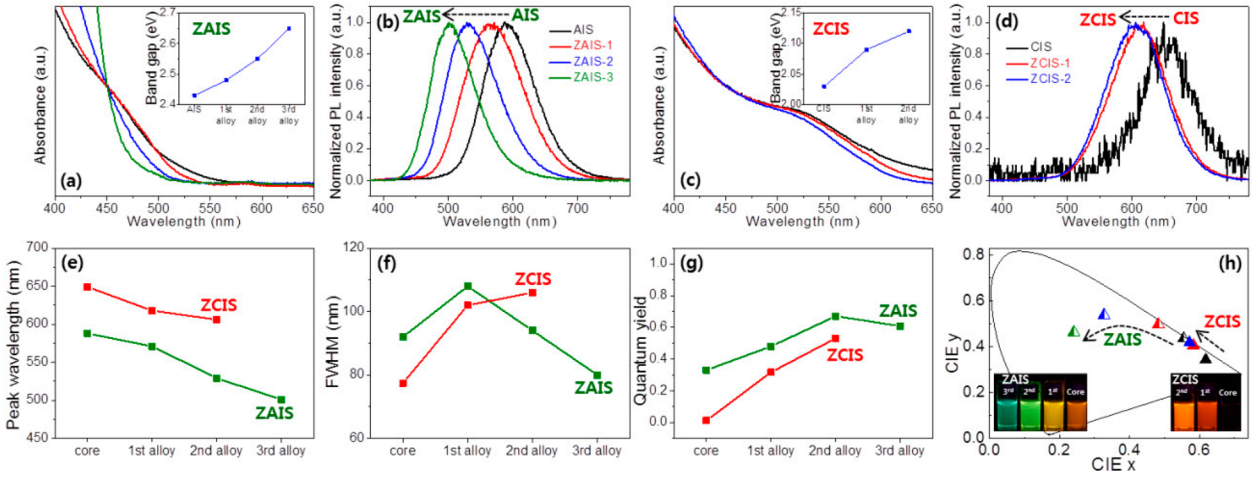


**Figure 1.** (a) UV−vis absorption (inset, band gap) and (b) normalized PL spectra of core and alloyed QDs of green ZAIS QDs. (c) UV−vis absorption (inset, band gap) and (d) normalized PL spectra of core and alloyed QDs of red ZCIS QDs. (e) Peak wavelength, (f) fwhm, (g) QY, and (h) CIE color coordinates of the green ZAIS and red ZCIS QDs as a function of alloying reaction step; (inset) photographs of emission of ZAIS and ZCIS QDs. The arrows in panels b, d, and h indicate the increased number of alloying reaction steps.

shell stock solution, consisting of 5.3 mmol of zinc stearate dissolved in 11.1 mmol of DDT and 16.7 mmol of ODE, was injected drop-wise at a rate of 2.0 mL/min into the ZCIS solution at each reaction temperature and reacted for 2 h. The crude red ZCIS QD solution was purified with centrifugation and stored in chloroform.

**Fabrication of Green−Red QD-based Single-Package DC-LED.** For the fabrication of a green−red QD-based single-package DC-LED, an InGaN blue LED ($\lambda_{max}$ = 445 nm) was used as an excitation source, and green ZAIS and red ZCIS QD solutions were prepared with optical density values of ∼3.0 at 450 nm in chloroform. The prepared green and red QD solutions were mixed with silicone binder and heated on a hot plate to evaporate the chloroform in the mixture at 90 °C for 30 min. These final green ZAIS and red ZCIS QD pastes were dispensed into an InGaN blue LED cup as a function of weight ratio. For the white DC-LED based on dual green and red QD color converters, mixtures of green emissive ZAIS, red emissive ZCIS, and silicone binder with various weight ratios of 28:1:82, 32:1:110, 40:1:160, 43:1:206, 50:1:283, and 54:1:445 were used for 2700, 3500, 4000, 5000, 6500, and 10 000 K, respectively.

**Characterization.**[32] The optical properties of the QDs were measured using a UV−vis spectrometer (S-3100, SINCO Co., Ltd.) for absorbance and a Xe-lamp and spectrophotometer (Darsa, PSI TRADING Co., Ltd.) for PL. The QY of the QDs was calculated with a commercial dye (Rhodamine 6G, QY = 95% in ethanol) as a reference by comparison of the integrated PL intensities. The structural properties of the QDs were investigated by X-ray diffraction (XRD) with Cu K$\alpha$ radiation (D-max 2500, Rigaku), and the size, shape, and lattice of the QDs were measured by transmission electron microscopy (TEM) with 200 kV (JEM-2100F, JEOL Ltd.). The optical properties of the DC-LEDs were measured in an integrated sphere by using a spectrophotometer (Darsapro-5000, PSI TRADING Co., Ltd.) with an applied current of 60 mA. The current dependence of the DC-LEDs was measured as a function of applied current from 10 to 120 mA with a 10 mA interval.

## RESULTS AND DISCUSSION

Both AIS and CIS QDs can be easily alloyed with ZnS to control the band gap and the wavelength of PL emission. Herein, ternary AIS and CIS core QDs and quaternary ZAIS and ZCIS core/shell-like alloy QDs are efficiently synthesized via a facile hot-injection route with multistep reactions of a low-temperature core synthesis and high-temperature alloying process.[43−45] As described in the Experimental Methods section, both the green ZAIS and the red ZCIS-alloyed QDs were synthesized by a three-step heating process involving core growth, a first alloying process, and a second alloying process. Figure 1a−d shows the typical UV−vis absorption and PL spectra of the core and alloyed QDs of both the green ZAIS QDs and red ZCIS QDs. It can be seen that the band gap and consequent emission energies of the ternary AIS and CIS QDs are significantly shifted to the blue wavelength by incorporating a Zn constituent, forming quaternary ZAIS and ZCIS core/shell-like alloy QDs. Here, the narrow bandgaps of the AIS and CIS QDs can be widened by forming an alloy (solid solution) with the ZnS shell with a wide bandgap through a bandgap engineering process. As a result of controlling the bandgap, the wavelengths of the absorption and emission spectra of the AIS and CIS semiconductor QDs are also altered in the desired manner by changing the chemical composition of the ZAIS and ZCIS alloyed QDs. We obtained the appropriate emission colors and color coordinates of the green and red-emitting QDs for their application to white DC-LEDs by optimizing the reaction temperature and time of the alloying step. As previously reported, it is considered that both the absorption and emission peaks of both green ZAIS and red ZCIS QDs move to a higher energy side as a result of not only the alloying process but also the etching process during the alloying step. It was reported that the blue shift of the alloying process is attributable to the formation of solid solutions with wider band gaps of ZnS, to the surface etching of I−III−VI QD during the shell growth and, consequently, to the reduction of effective core QD size.[46,47]

Here, the variations of the peak wavelength, fwhm, QY, and CIE color coordinates of the green ZAIS and red ZCIS QDs are displayed as a function of the shelling, alloying, or both reaction step of the ternary AIS or CIS cores and ZnS (Figure 1e−h). The peak wavelengths of the last alloyed green ZAIS and red ZCIS QDs reached 501 and 606 nm with fwhm values of 81 and 106 nm, respectively. The PL QYs of all the ZAIS and ZCIS alloyed QDs are enhanced by adding ZnS to the core QDs, irrespective of the I−III−VI core material, as previously reported.[2,11] The PL QYs of the resultant green ZAIS and red ZCIS QD samples reach about 0.61 and 0.53, respectively. In particular, the PL QYs of the ZCIS alloy QDs were almost 41 times higher than those of their CIS core counterparts, whereas the ZAIS alloyed QDs show QYs enhanced about 1.8 times


DOI: 10.1021/acsami.5b00664
ACS Appl. Mater. Interfaces 2015, 7, 7342−7350

compared to the original bare AIS cores. These significant differences of PL QY enhancement levels may be understood based on the earlier hypothesis that AIS core QDs have lower surface defect density than do CIS core QDs. As explained in our previous publications,[18,32] if the passivation of the core-alloy surface by the ZnS shell filled most of the surface states present for all the ZAIS and ZCIS QDs, the surface state-related nonradiative recombination would no longer be dominant; then, only the intragap internal states and their concentrations would govern the radiative recombination and determine its efficiency, respectively, resulting in similar values of PL QY for ZAIS or ZCIS alloyed QDs and even resulting in a slight decrease of PL QY of the ZAIS alloyed QD after multiple ZnS injection reactions. These values indicate that the resultant green ZAIS and red ZCIS QDs show adjustable peak wavelengths and color coordinates with proper QY and wide fwhm for application in green and red color converting white DC-LEDs.

The formation of alloyed crystals in both the green ZAIS and red ZCIS QDs samples can be seen in the XRD measurements and via HR-TEM observation. As shown in Figure 2, the XRD

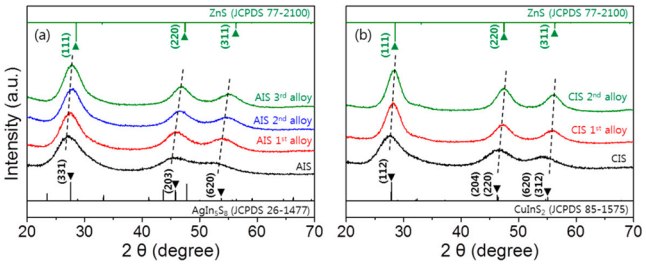


**Figure 2.** (a) XRD patterns of AIS core and multiple alloyed ZAIS QD samples, (b) XRD patterns of CIS core and multiple alloyed ZCIS QD samples; (green ▲) the three main peaks of bulk cubic ZnS and (black ▼) the three main broad peaks of the AIS and CIS QDs.

patterns also indicate that three broad peaks exist in all core and multiple alloyed QD samples. As previously reported, the three broad peaks are a typical feature in the XRD patterns of I–III–VI and ZnS alloyed QDs.[2,48−50] The XRD data also indicate that the three broad peaks of the cubic $AgIn_5S_8$ and tetragonal $CuInS_2$ QD samples have shifted to a higher angle after ZnS alloying. Each shifted peak is located between the corresponding peaks of the bulk cubic ZnS and the c-$AgIn_5S_8$ and t-$CuInS_2$, respectively. These facts also confirm that the obtained ZAIS and ZCIS QD powders are not a mixture of ZnS and AIS or CIS but are almost solid-solutions of ZnS–AIS or ZnS–CIS. Figure 3 provides HR-TEM images of the green ZAIS and red ZCIS QDs prepared at 120, 180, 220, and 220 °C and 160, 230, and 230 °C, respectively, at the very beginning of the focus stage of the HR-TEM measuring process, that is, at a focus time of less than 10 s. Similar to the TEM images used in previous publications, TEM images of both ZAIS and ZCIS QDs reveal that the oval shape single crystals have a clear single and continuous lattice fringe with interplanar spacing of 0.322 and 0.312 nm for the ZAIS and ZCIS QD, respectively.[50,51] This reveals the highly crystalline nature of the as-synthesized ZAIS and ZCIS QDs. The measurements of the single lattice spacing, and no evidence of the formation of an interface between I–III–VI and ZnS in both green ZAIS and red ZCIS QDs, also confirm that these two samples were the result of the coherent epitaxial growth of shells or solid-solutions, irrespective of the

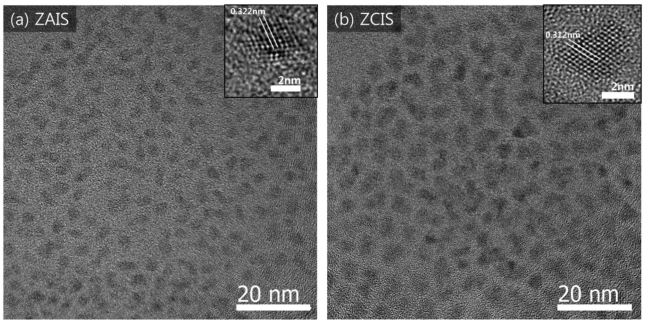


**Figure 3.** (a) Low- and (inset) high-magnification TEM images of triple-alloyed ZAIS QD and (b) low- and (inset) high-magnification TEM images of double-alloyed ZCIS QD.

crystal phases of the core AIS and CIS QDs. The average diameters of the ZAIS- and ZCIS-alloyed QDs from the TEM measurements were found to be approximately 3.9 and 4.4 nm, respectively.

Table 2 summarizes the optical properties and synthetic conditions of the three green ZAIS alloyed QDs and the three

**Table 2. Optical Properties of ZAIS and ZCIS Alloyed QDs**

| sample | final alloy reaction temperature (°C) | CIE $x$ | CIE $y$ | peak wavelength (nm) | fwhm (nm) | QY |
|---|---|---|---|---|---|---|
| ZAIS series | 210 | 0.347 | 0.554 | 526 | 88 | 0.75 |
| | 220 | 0.241 | 0.464 | 501 | 81 | 0.61 |
| | 230 | 0.225 | 0.388 | 491 | 89 | 0.42 |
| ZCIS series | 220 | 0.577 | 0.413 | 614 | 104 | 0.44 |
| | 230 | 0.572 | 0.418 | 606 | 106 | 0.53 |
| | 240 | 0.545 | 0.447 | 589 | 98 | 0.57 |

red ZCIS alloyed QDs in order to show the possibility of finely tuning the peak wavelength and determining a good green and red candidate for wide-band QD-based RGB tricolor white LED. The peak wavelengths of the three green ZAIS alloyed QDs are located between 491 and 526 nm, with broad fwhm values over 81 nm. Otherwise, the peak wavelengths of the three red ZCIS alloyed QDs are located at 589 and 614 nm, with broader fwhm values over 98 nm (Figure 4a,b).

In this experiment, even though the emission peaks of the broad-bandwidth alloyed QDs are not in general easily tuned to the wavelength by controlling the core size of the QDs, here, the fine-tuning of the peak wavelength (Figure 4a,b) and the CIE color coordinates (Figure 4c) can be successfully performed by controlling the degree of alloying capability using different alloying temperatures and reaction times (i.e., amounts of ZnS). As has been previously reported in many publications,[52,53] the retained broad FWHMs (>80 nm) and the less tunable size-selective effect of the emission spectra suggest that the green ZAIS alloyed QDs and red ZCIS alloyed QDs contain many D–A transitions, free-to-bound, or bound-to-free transitions that contribute to the wide range of radiative transitions. To study the suitability of the broad-bandwidth green ZAIS and red ZCIS alloyed QDs as color-conversion materials for use in high color-quality white DC-LEDs, we compared three green and three red emitted samples; then, we selected one green (501 nm) and one red (606 nm) QD candidate after considering both the high QY and the proper


DOI: 10.1021/acsami.5b00664
ACS Appl. Mater. Interfaces 2015, 7, 7342−7350

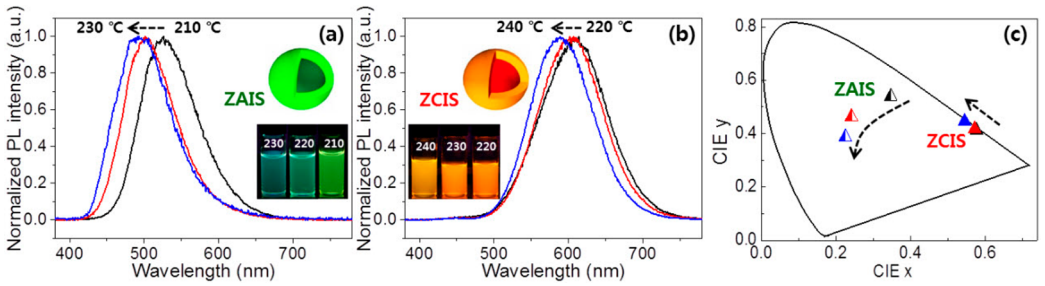


**Figure 4.** Emission PL spectra of (a) ZAIS and (b) ZCIS. (c) CIE color coordinates of three green ZAIS and three red ZCIS-alloyed QDs under various final temperatures for each ZAIS (210, 220, and 230 °C) and ZCIS (220, 230, and 240 °C) QD. (Insets) Schematic diagrams of QDs and photographs of the emissions of the ZAIS and ZCIS QDs. The arrows indicate the increase in the final reaction temperature.

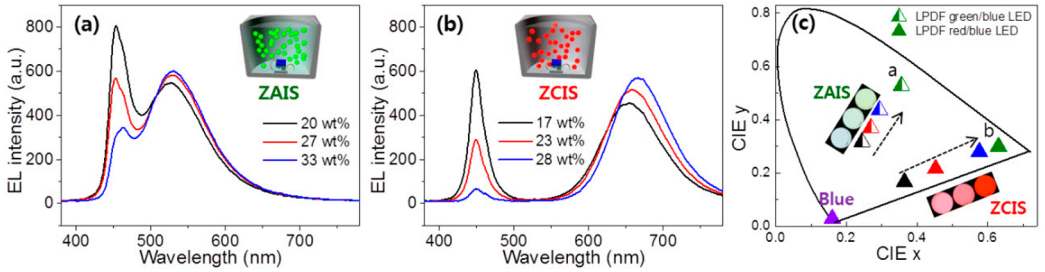


**Figure 5.** EL emission spectra of partially converted (a) green ZAIS QD and (b) red ZCIS QD-based LEDs as a function of the QD concentration; (insets) schematic diagrams of QD-based LEDs. (c) CIE chromaticity coordinates of green ZAIS QD and red ZCIS QD-based two-color QD LEDs as a function of QD concentration; a and b indicate the color coordinates from the LPDF-capped dicolor spectrum of the green/blue and red/blue QD-based LEDs, respectively; (inset) photographs of the emission of ZAIS QD and ZCIS QD-based dicolor LEDs. Arrows indicate the increase in the concentration of QDs.

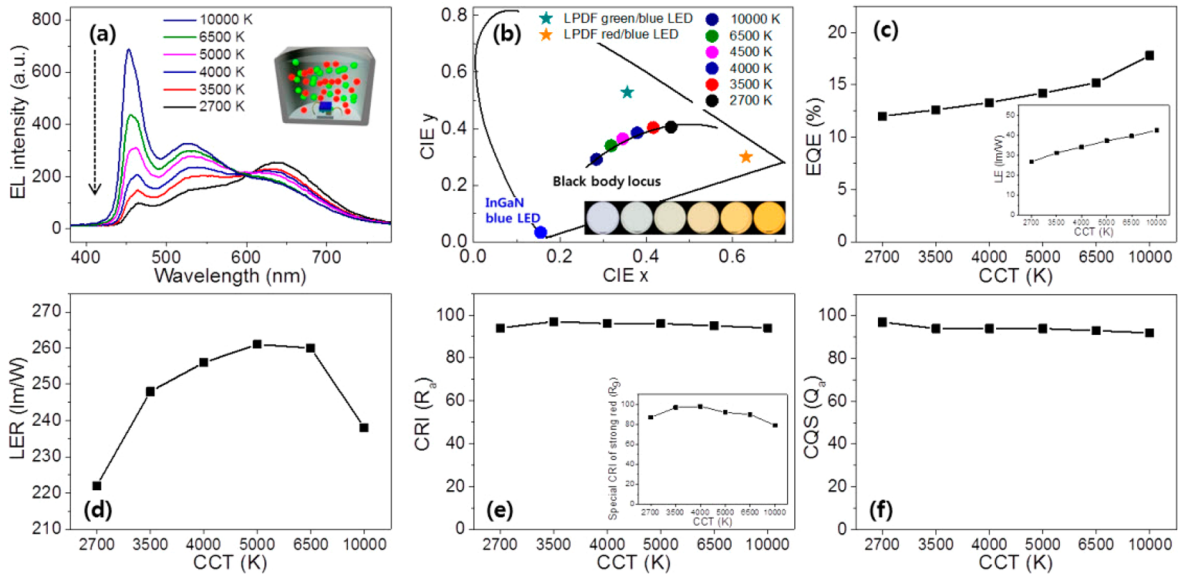


**Figure 6.** (a) EL emission spectra of six I–III–VI QD-based tricolor white LEDs as a function of the CCTs; arrow indicates the decrease of CCT. (b) CIE chromaticity coordinates of mixed green ZAIS and red ZCIS QD-based tricolor white LEDs with the variation of CCT; stars (★) indicates the color coordinates of monochromatic green and red peaks in the filtered EL white spectrum of the LPDF-capped, I–III–VI QD-based dicolor green/blue and red/blue LEDs, respectively; (inset) photographs of emission of ZAIS and ZCIS QD-based white DC-LEDs with a decrease in the CCT from left to right. (c) EQE and LE, (d) LER, (e) CRI and $R_9$, and (f) CQS of six I–III–VI QD-based tricolor white LEDs as a function of the CCT.

emission wavelength to cover the cyan gap and the proper red region in the white spectrum when fabricating the tricolor single package white DC-LED.

Compared to the narrow band emissions of commercialized CdSe/ZnS-based QDs (fwhm <30 nm), these broad-bandwidth emissions of the green ZAIS and red ZCIS alloyed QDs could have desirable characteristics for realizing ultrahigh color rendering white LEDs. Figure 5a,b shows the changes of the electroluminescent (EL) emission spectra of partially converted green and red QD-based LEDs were prepared with three concentrations in each case in a silicone binder (ZAIS, 20, 27, and 33 wt %; ZCIS, 17, 23, and 28 wt %) at an equal-current


DOI: 10.1021/acsami.5b00664
ACS Appl. Mater. Interfaces 2015, 7, 7342–7350

condition (60 mA). When the concentration of the ZAIS-alloyed QDs is increased, the intensity of the blue emission from the InGaN LED chip decreases, while that of the green emission of the ZAIS-alloyed QD increases slightly due to the low transmission of blue light and the efficient Förster resonant energy transfer (FRET) of inter-QD at a high concentration of QDs. Figure 5c shows the variations of the CIE color coordinates of the EL spectra of the blue and green ZAIS (or red ZCIS) alloyed QD emitting dicolor LEDs as a function of the concentration of both green and red QDs. As the concentration of the ZAIS alloyed QD is increased, the CIE chromaticity coordinates shift from those of blue LED ($x$ = 0.16, $y$ = 0.03) to those of the pure green emitting ZAIS alloyed QD ($x$ = 0.37, $y$ = 0.53; Figure 5c, a). Similarly, the red emission of the ZCIS alloyed QDs decreases with the increase of the ZCIS alloyed QD concentrations, while the blue emission decreases as shown in Figure 5b. Here, the color coordinates of the pure green and red spectrum were calculated from the green and red spectrum from the long-wave pass dichroic filter (LPDF) capped dicolor spectrum of green/blue and red/blue LED, respectively.[54] Also, the CIE color coordinates of the blue and red emitting LEDs move from those of blue to those of the red ZCIS alloyed QD ($x$ = 0.63, $y$ = 0.30; Figure 5c, b) when the QD concentration is increased in the LED package. Therefore, by controlling the ratio and amounts of the green ZAIS and red ZCIS alloyed QDs in the silicone resin, the color coordinates of white LEDs with green ZAIS alloyed and red ZCIS alloyed QDs can reproduce any of the CIE color coordinates within the color gamut, which is triangularly defined by the color points of red, green, and blue. Moreover, a wide-bandwidth white DC-LED can be obtained as a set of six CCTs along Planckian locus radiation, although the reproduction area of the triangle is relatively small compared to that of the narrow-bandwidth QD white LEDs.

We fabricated six different white LEDs with the selected concentration of green and red QDs on a chip-type LED using proper concentration ratio of green QD, red QD, and silicone binder (in the Experimental Methods section). Figure 6a illustrates the spectral changes of the six I–III–VI QD-based white LEDs as a function of the CCTs using one green ZAIS and one red ZCIS QD. As previously reported, the intensity of the red part of spectrum in each sample of white light gradually increased with the decrease of the CCT of the white color. In contrast, the blue-green part of spectrum increased with the increase of the CCT. Figure 6b also shows the change of the CIE color coordinates of the six different single-package white LEDs at 60 mA (rated current) with CCTs of 2700, 3500, 4000, 5000, 6500, and 10 000 K. These figures indicate that the color coordinates of the white LEDs move from warm white to cool white with the increase of the concentration ratio between the green and red QDs. In addition, the figures of merit for vision performance and color performance, such as external quantum efficiency (EQE), LE, the luminous efficacy of radiation (LER), CRI, CQS, and $R_9$ were measured and calculated from the SPDs of the six white lights at an applied current of 60 mA (rated current of LED; Figure 6c–f). As previously reported,[54–56] CQS and $R_9$ were proposed as a complementary color rendition metric to compensate for the insufficient capability of the CRI to reproduce saturated blue, green, and red colors. Here, Figure 6c indicates that the EQE of the I–III–VI QD-based tricolor white LED decreases slowly with CCT decrease, in a trend similar to that of the phosphor-based tricolor white LED, owing to the various increased energy loss mechanisms, such as absorption, scattering, and screening loss, with the increase of green and red concentration in the silicone resin. Compared to the trend of EQE, LE decreased in slightly different manner from the decrease of the CCT because of the additional decreased effect of the low eye sensitivity of the enhanced bluish and reddish color at high (10 000 K) and low CCT (2700 K; Figure 6c, inset).

The results also show that the CRI ($R_a$) and CQS ($Q_a$) values are very high, with values of more than 93 for all LED lamps with six different CCTs. $R_9$ values over 79 are high enough to render pure red colors of reflected light from any object. Especially, the maximum values of CRI and CQS reach over 97 and 94, respectively, for white colors between 3500 and 6500 K. These ultrahigh values of CRI, $R_9$, and CQS confirm that the SPD shapes of the I–III–VI QD-based RGB white LED systems with wide-bandwidth green and red QDs are close to those of the radiation spectrum of sunlight over 5000 K and candlelight less than 5000 K. It can also be speculated that this outcome indicates that a white-by-UV LED system including a wide bandwidth of blue phosphor is not always necessary for high color rendering white LED lamps, owing to the closing of the cyan gap between the blue and green peak via the use of a wide-bandwidth of green ZAIS QD.

To explain the increasing possibility of closing the cyan gap, PL spectra of ZAIS and ZCIS QDs were measured under different excitation wavelengths of a Xe lamp between 440 and 460 nm with 5 nm intervals. Because the emission spectrum of the blue LED has a peak wavelength of 450 nm with a fwhm of ~23 nm, it is necessary to analyze the effect of the wavelength of narrow band blue on the emission spectrum of green or red QDs. Figure 7a,b indicates that the green emission peaks of the ZAIS QDs are shifted to a reddish color with an increase of the excitation wavelength, but the red emission peaks of ZCIS QDs are not moved and are located at the same wavelength irrespective of the excitation wavelengths within the blue LED spectrum. The real peak broadness of the green emissive ZAIS

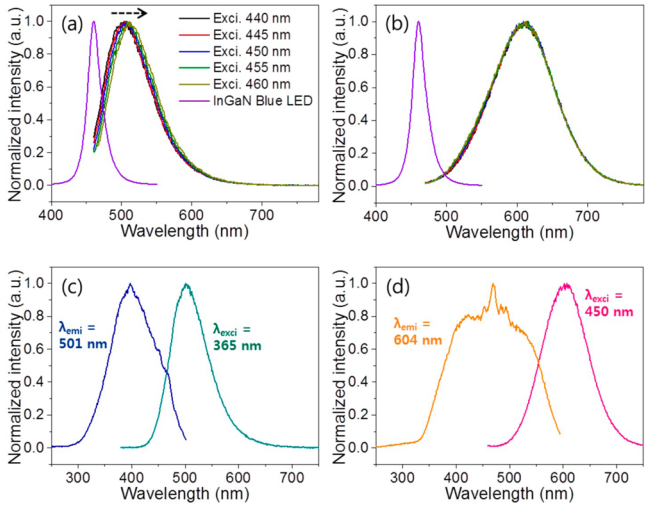


**Figure 7.** (a) Emission spectra of green emitting ZAIS QDs excited by a Xe lamp between 440 and 460 nm with 5 nm intervals. (b) Emission spectra of red emitting ZCIS QDs excited by a Xe lamp between 440 and 460 nm with 5 nm intervals. The excitation and PL emission spectra of (c) green emitting ZAIS and of (d) red emitting ZCIS QDs selected for fabricating QD-based white DC-LEDs. The arrow indicates the increase in the incident excitation wavelength of the ZAIS QDs.



DOI: 10.1021/acsami.5b00664
ACS Appl. Mater. Interfaces 2015, 7, 7342–7350

QDs excited by the blue LED hence is slightly larger than that excited by the Xe lamp, owing to the wider fwhm of the blue LED (~23 nm) than the Xe lamp (~8 nm). This broadening of the green emission by the blue LED is ascribed to the overlapped excitation peak and the PL emission peak of the ZAIS green QDs at the wavelength of ~450 nm (Figure 7c). However, no broadening of red ZCIS QDs is observed by the excitation of the blue LED, owing to the absence of overlapping between excitation and emission peaks at the wavelength of 450 nm (Figure 7d). Finally, the emission peaks excited by the blue LED light at the shorter wavelength (~440 nm) provide the possibility of closing the cyan gap between blue LED and green ZCIS QD emissions. For this reason, the CRIs, $R_9$s, and CQSs of the I−III−VI QD-based RGB white LED systems displayed ultrahigh values compared to those of I−III−VI based QD white DC-LEDs in various previous works.[10,35−41] Therefore, the RGB positions and combined broad-bandwidths of the transmitted blue peaks and the emitted green and red peaks in the DC-LED spectra of the six different I−III−VI QD-based LEDs with different CCTs make it possible to utilize green ZAIS and red ZCIS QDs in high color quality white LEDs.

Furthermore, the detailed EL properties of the five different CCT, II−I−III-VI alloyed QD-based, tricolor white DC-LEDs are compared with increases of the applied current. Figure 8a,b

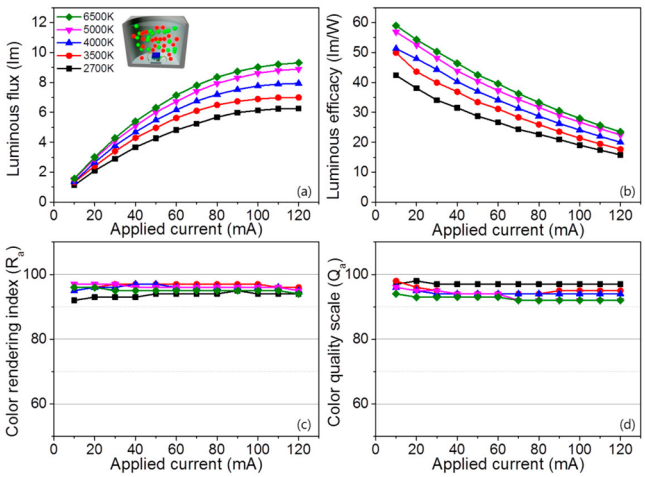


**Figure 8.** (a) Luminous flux (lm), (b) LE (lm/W), (c) CRI ($R_a$), and (d) CQS ($Q_a$) of six I−III−VI QD-based tricolor white LEDs as a function of applied current.

shows that, with an increase in the applied current from 10 to 120 mA, the luminous flux and LE of the 6500 K I−III−VI QD-based LED are higher than those of the other CCT LEDs. Figure 8b also shows that the LEs of the I−III−VI QD-based LEDs are 38, 44, 48, 53, and 54 lm/W at 20 mA with CCT of 2700, 3500, 4000, 5000, and 6500 K, respectively. The relative LE values shown in Figure 8b indicate that the decreasing gradients in the LE of all five I−III−VI QD-based LEDs behave in similar to the increase in the applied current. This similar decreasing trend was caused by the similar combined effects of the similar thermal degradation of the green ZAIS alloyed and red ZCIS alloyed QDs and the same current degradation of the blue LED chip with the increase in the current. Furthermore, Figure 8c,d shows the CRI ($R_a$) and CQS ($Q_a$) values of the broad band II−I−III-VI QD-based LEDs with five CCTs as a function of applied current. The data in the figure indicate that the variation of the CRI and CQS for all four II−I−III−VI QD-based core−shell like alloyed LEDs is relatively low in spite of the increase in the current; the II−I−III-VI QD-based white LEDs are relatively stable under typical LED ranges of applied current. Ultrahigh color qualities, such as CRI and CQS, are thus maintained at values above 90, even at high applied current.

## CONCLUSIONS

In this study, we successfully prepared various wide-bandwidth green ZAIS and red ZCIS QDs with tunable PL emissions in the wavelength range of green to amber emission by ZAIS QDs and yellow to red emission by ZCIS QDs, respectively, using a multistep hot-injection method. This method uses a facile approach of low-temperature core growth and high-temperature alloyed reaction to enhance the possibility of the formation of a core−shell-like solid solution between the AIS and CIS cores and the ZnS shell. If the appropriate AIS and CIS core growth and ZnS alloying temperature are selected, the proposed method can easily be employed to achieve the preparation of the alloyed QDs, select a tunable peak wavelength, broaden the fwhm, and enhance the QYs of the green ZAIS and red ZCIS QDs. After triple ZnS alloying over the AIS core and double ZnS alloying over the CIS core, green ZAIS and red ZCIS QDs reached PL QY values as high as 0.61 and 0.53, respectively, and PL FWHMs as broad as 81 and 106 nm, respectively. Furthermore, the overlapped excitation peak and PL emission peak of ZAIS QDs provides the possibility of broadening the bandwidth of the PL emission peak of ZAIS QDs that are excited by a blue emission of an InGaN LED with a moderate fwhm (~23 nm). Therefore, it is emphasized that our green ZAIS and red ZCIS QDs are comparable in color tunability and fwhm, and only slightly inferior in QY value, to the best AIS and CIS-based QDs available to date.

Through additional elaborate research, a combination of broad fwhm green ZAIS and red ZCIS QDs of tricolor DC-LEDs can provide the potential to close the cyan gap of the white spectrum in phosphor-based white DC-LEDs if the LE and stability are enhanced over the level of inorganic, phosphor-based, tricolor DC-LEDs. A careful evaluation of the LE, LER, CRI, $R_9$, and CQS of the RGB tricolor white DC-LED, including green ZAIS and red ZCIS QDs with a blue LED, demonstrated that the green ZAIS and red ZCIS QDs are feasible candidates as color-converting materials in ultrahigh color quality white LEDs at various CCTs. Regarding overall color performance, a green ZAIS and red ZCIS QD-based tricolor single-package white DC-LED offers excellent color quality (CRI = 94−97, CQS = 93−97, and $R_9$ = 87−98), moderate LE performance (LE = 26.7, 31.2, 34.1, 37.2, and 39.6 lm/W for 2700, 3500, 4000, 5000, and 6500 K at an applied current of 60 mA). Therefore, our broad fwhm, color-tunable ZAIS and ZCIS QDs, which are made of nontoxic elements, have demonstrated potential for applications involving single-package, tricolor, white DC-LEDs with ultrahigh color qualities.

## AUTHOR INFORMATION

### Corresponding Author

*E-mail: yrdo@kookmin.ac.kr. Phone: +82-2-910-4893. Fax: +82-2-910-4415.

### Notes

The authors declare no competing financial interest.



DOI: 10.1021/acsami.5b00664
ACS Appl. Mater. Interfaces 2015, 7, 7342−7350

## ■ ACKNOWLEDGMENTS

This work was supported by a National Research Foundation of Korea (NRF) grant funded by the Korean government (Ministry of Science, ICT & Future Planning (MSIP), No. 2011-0017449).

## ■ REFERENCES

(1) Li, L.; Reiss, P. One-Pot Synthesis of Highly Luminescent InP/ZnS Nanocrystals without Precursor Injection. *J. Am. Chem. Soc.* **2008**, *130*, 11588−11589.
(2) Torimoto, T.; Adachi, T.; Okazaki, K.; Sakuraoka, M.; Shibayama, T.; Ohtani, B.; Kudo, A.; Kuwabata, S. Facile synthesis of ZnS-$AgInS_2$ Solid Solution Nanoparticles for a Color Adjustable Luminophore. *J. Am. Chem. Soc.* **2007**, *129*, 12388−12389.
(3) Uematsu, T.; Doi, T.; Torimoto, T.; Kuwabata, S. Preparation of Luminescent $AgInS_2$−$AgGaS_2$ Solid Solution Nanoparticles and Their Optical Properties. *J. Phys. Chem. Lett.* **2010**, *1*, 3283−3287.
(4) Allen, P. M.; Bawendi, M. G. Ternary I-III-VI Quantum Dots Luminescent in the Red to Near-Infrared. *J. Am. Chem. Soc.* **2008**, *130*, 9240−9241.
(5) Santra, P. K.; Nair, P. V.; Thomas, K. G.; Kamat, P. V. $CuInS_2$-Sensitized Quantum Dot Solar Cell. Electrophoretic Deposition, Excited-State Dynamics, and Photovoltaic Performance. *J. phys. Chem. Lett.* **2013**, *4*, 722−729.
(6) Sasamura, T.; Okazaki, K.; Kudo, A.; Kuwabata, S.; Torimoto, T. Photosensitization of ZnO Rod Electrodes with $AgInS_2$ Nanoparticles and ZnS-$AgInS_2$ Solid Solution Nanoparticles for Solar Cell Applications. *RSC Adv.* **2012**, *2*, 552−559.
(7) Oh, J. H.; Lee, K. H.; Yoon, H. C.; Yang, H.; Do, Y. R. Color-by-blue Display Using Blue Quantum Dot Light-Emitting Diodes and Green/Red Color Converting Phosphors. *Opt. Express* **2014**, *22*, A511−A520.
(8) Lee, S. H.; Lee, K. H.; Jo, J. H.; Park, B.; Kwon, Y.; Jang, H. S.; Yang, H. Remote-Type, High-Color Gamut White Light-Emitting Diode based on InP Quantum Dot Color Converters. *Opt. Mater. Express* **2014**, *4*, 1297−1302.
(9) Kim, J. H.; Lee, K. H.; Jo, D. H.; Lee, Y.; Hwang, J. Y.; Yang, H. CuInGaS Quantum Dot Composition-Dependent Device Performance of Electrically Driven Light-Emitting Diodes. *Appl. Phys. Lett.* **2014**, *105*, 133104.
(10) Song, W. S.; Lee, S. H.; Yang, H. Fabrication of Warm, High CRI White LED Using Non-cadmium Quantum Dots. *Opt. Mater. Express* **2013**, *3*, 1468−1473.
(11) Song, W. S.; Yang, H. Efficient White-Light-Emitting Diodes Fabricated from Highly Fluorescent Copper Indium Sulfide Core/Shell Quantum Dots. *Chem. Mater.* **2012**, *24*, 1961−1967.
(12) Zaban, A.; Mićić, O. I.; Gregg, B. A.; Nozik, A. J. Photosensitization of Nanoporous $TiO_2$ Electrodes with InP Quantum Dots. *Langmuir* **1998**, *14*, 3153−3156.
(13) Arici, E.; Sariciftci, N. S.; Meissner, D. Hybrid Solar Cells Based on Nanoparticles of $CuInS_2$ in Organic Matrices. *Adv. Funct. Mater.* **2003**, *13*, 165−171.
(14) Smith, A. M.; Dave, S.; Nie, S.; True, L.; Gao, X. Multicolor Quantum Dots for Molecular Diagnostics of Cancer. *Expert Rev. Mol. Diagn.* **2006**, *6*, 231−244.
(15) Uematsu, T.; Taniguchi, S.; Torimoto, T.; Kuwabata, S. Emission Quench of Water-Soluble ZnS−$AgInS_2$ Solid Solution Nanocrystals and Its Application to Chemosensors. *Chem. Commun.* **2009**, *48*, 7485−7487.
(16) Chen, B.; Zhong, G.; Zhang, W.; Tan, Z.; Li, Y.; Yu, C.; Zhai, T.; Bando, Y.; Yang, S.; Zou, B. High Emissive and Color-Tunable $CuInS_2$-Based Colloidal Semiconductor Nanocrystals: Off-Stoichiometry Effects and Improved Electroluminescence Performance. *Adv. Funct. Mater.* **2012**, *22*, 2081−2088.
(17) Shi, A.; Wang, X.; Meng, X.; Liu, X.; Haibo, Li.; Zhao, J. Temperature-Dependent Photoluminescence of $CuInS_2$ Quantum Dots. *J. Lumin.* **2012**, *132*, 1819−1823.
(18) Park, Y. J.; Oh, J. H.; Han, N. S.; Yoon, H. C.; Park, S. M.; Do, Y. R.; Song, J. K. Photoluminescence of Band Gap States in $AgInS_2$ Nanoparticles. *J. Phys. Chem. C* **2014**, *118*, 25677−25683.
(19) Mao, B.; Chuang, C. H.; Wang, J.; Burda, C. Synthesis and Photophysical Properties of Ternary I−III−VI $AgInS_2$ Nanocrystals: Intrinsic versus Surface States. *J. Phys. Chem. C* **2011**, *115*, 8945−8954.
(20) Tu, C. C.; Hoo, J. H.; Böhringer, K. F.; Lin, L. Y.; Cao, G. Red-emitting Silicon Quantum Dot Phosphors in Warm White LEDs with Excellent Color Rendering. *Opt. Express* **2014**, *22*, A276−A281.
(21) Zhong, P.; He, G.; Zhang, M. Optimal Spectra of White Light-Emitting Diodes Using Quantum Dot Nanophosphors. *Opt. Express* **2012**, *20*, 9122−9134.
(22) Song, W. S.; Kim, H. J.; Kim, Y. S.; Yang, H. Synthesis of $Ba_2Si_3O_8$: $Eu^{2+}$ Phosphor for Fabrication of White Light-Emitting Diodes Assisted by ZnCdSe/ZnSe Quantum Dot. *J. Electrochem. Soc.* **2010**, *157*, J319−J323.
(23) Jang, E.; Jun, S.; Jang, H.; Lim, J.; Kim, B.; Kim, Y. White-Light-Emitting Diodes with Quantum Dot Color Converters for Display Backlights. *Adv. Mater.* **2010**, *22*, 3076−3080.
(24) Erdem, T.; Nizamoglu, S.; Sun, X. W.; Demir, H. V. A Photometric Investigation of Ultra-Efficient LEDs with High Color Rendering Index and High Luminous Efficacy Employing Nanocrystal Quantum Dot Luminophores. *Opt. Express* **2010**, *18*, 340−347.
(25) Gosnell, J. D.; Rosenthal, S. J.; Weiss, S. M. White Light Emission Characteristics of Polymer-Encapsulated CdSe Nanocrystal Films. *IEEE Photonics Technol. Lett.* **2010**, *22*, 541−543.
(26) Wang, X. B.; Yan, X. S.; Li, W. W.; Sun, K. Doped Quantum Dots for White-Light-Emitting Diodes without Reabsorption of Multiphase Phosphors. *Adv. Mater.* **2012**, *24*, 2742−2747.
(27) Liang, R.; Yan, D.; Tian, R.; Yu, X.; Shi, W.; Li, C.; Wei, M.; Evans, D. G.; Duan, X. Quantum Dots-Based Flexible Films and Their Application as the Phosphor in White Light-Emitting Diodes. *Chem. Mater.* **2014**, *26*, 2595−2600.
(28) Mutlugun, E.; Hernandez-Martinez, P. L.; Eroglu, C.; Coskun, Y.; Erdem, T.; Sharma, V. K.; Unal, E.; Panda, S. K.; Hickey, S. G.; Gaponik, N. Large-Area (over 50 cm × 50 cm) Freestanding Films of Colloidal InP/ZnS Quantum Dots. *Nano Lett.* **2012**, *12*, 3986−3993.
(29) Kim, K.; Jeong, S.; Woo, J. Y.; Han, C. S. Successive and Large-Scale Synthesis of InP/ZnS Quantum Dots in a Hybrid Reactor and Their Application to White LEDs. *Nanotechnology* **2012**, *23*, 065602.
(30) Kwon, K. H.; Im, W. B.; Jang, H. S.; Yoo, H. S.; Jeon, D. Y. Luminescence Properties and Energy Transfer of Site-Sensitive $Ca_{6-x-y}Mg_{x-z}(PO_4)_4$:$Eu_y^{2+}$,$Mn_z^{2+}$ Phosphors and Their Application to Near-UV LED-Based White LEDs. *Inorg. Chem.* **2009**, *48*, 11525−11532.
(31) Kimura, N.; Sakuma, K.; Hirafune, S.; Asano, K.; Hirosaki, N.; Xie, R. J. Extrahigh Color Rendering White Light-Emitting Diode Lamps Using Oxynitride and Nitride Phosphors Excited by Blue Light-Emitting Diode. *Appl. Phys. Lett.* **2007**, *90*, 051109.
(32) Hong, S. P.; Park, H. K.; Oh, J. H.; Yang, H.; Do, Y. R. Comparisons of The Structural and Optical Properties of o-$AgInS_2$, t-$AgInS_2$, and c-$AgIn_5S_8$ Nanocrystals and Their Solid-Solution Nanocrystals with ZnS. *J. Mater. Chem.* **2012**, *22*, 18939−18949.
(33) Song, W. S.; Kim, J. H.; Lee, J. H.; Lee, H. S.; Do, Y. R.; Yang, H. Synthesis of Color-Tunable Cu−In−Ga−S Solid Solution Quantum Dots with High Quantum Yields for Application to White Light-Emitting Diodes. *J. Mater. Chem.* **2012**, *22*, 21901−21908.
(34) Song, W. S.; Yang, H. Fabrication of White Light-Emitting Diodes Based on Solvothermally Synthesized Copper Indium Sulfide Quantum Dots as Color Converters. *Appl. Phys. Lett.* **2012**, *100*, 183104.
(35) Chen, B.; Zhou, Q.; Li, J.; Zhang, F.; Liu, R.; Zhong, H.; Zou, B. Red Emissive $CuInS_2$-based Nanocrystals: A Potential Phosphor for Warm White Light-Emitting Diodes. *Opt. Express* **2013**, *21*, 10105−10110.
(36) Aboulaich, A.; Michalska, M.; Schneider, R.; Potdevin, A.; Deschamps, J.; Deloncle, R.; Chadeyron, G.; Mahiou, R. Ce-Doped YAG Nanophosphor and Red Emitting $CuInS_2$/ZnS Core/Shell


DOI: 10.1021/acsami.5b00664
*ACS Appl. Mater. Interfaces* 2015, 7, 7342−7350

Quantum Dots for Warm White Light-Emitting Diode with High Color Rendering Index. *ACS Appl. Mater. Interface* **2014**, *6*, 252−258.
(37) Chen, B.; Zhong, H.; Wang, M.; Liu, R.; Zou, B. Integration of $CuInS_2$-based Nanocrystals for High Efficiency and High Colour Rendering White Light-Emitting Diodes. *Nanoscale* **2013**, *5*, 3514−3519.
(38) Huang, B.; Dai, Q.; Zhuo, N.; Jiang, Q.; Shi, F.; Wang, H.; Zhang, H.; Liao, Chen; Cui, Y.; Zhang, J. Bicolor Mn-doped $CuInS_2$/ZnS Core/Shell Nanocrystals for White Light-Emitting Diode with High Color Rendering Index. *J. Appl. Phys.* **2014**, *116*, 094303.
(39) Chuang, P. H.; Lin, C. C.; Liu, R. S. Emission-Tunable $CuInS_2$/ZnS Quantum Dots: Structure, Optical Properties, and Application in White Light-Emitting Diodes with High Color Rendering Index. *ACS. Appl. Mater. Interfaces* **2014**, *6*, 15379−15387.
(40) Sun, C.; Zhang, Y.; Wang, Y.; Liu, W.; Kalytchuk, S.; Kershaw, S. V.; Zhang, T.; Zhang, X.; Zhao, J.; Yu, W. W.; Rogach, A. L. High Color Rendering Index White Light Emitting Diodes Fabricated from a Combination of Carbon Dots and Zinc Copper Indium Sulfide Quantum Dots. *Appl. Phys. Lett.* **2014**, *104*, 261106.
(41) Kim, J. H.; Yang, H. White Lighting Device from Composite Films Embedded with Hydrophilic Cu(In, Ga)$S_2$/ZnS and Hydrophobic InP/ZnS Quantum Dots. *Nanotechnology* **2014**, *25*, 225601.
(42) Sheng, Y.; Wei, J.; Liu, B.; Peng, L. A Facile Route to Synthesize CdZnSe Core−Shell-like Alloyed Quantum Dots via Cation Exchange Reaction in Aqueous System. *Mater. Res. Bull.* **2014**, *57*, 67−71.
(43) Torimoto, T.; Ogawa, S.; Adachi, T.; Kameyama, T.; Okazaki, K.; Shibayama, T.; Kudo, A.; Kuwabata, S. Remarkable Photoluminescence Enhancement of ZnS−$AgInS_2$ Solid Solution Nanoparticles by Post-Synthesis Treatment. *Chem. Commun.* **2010**, *46*, 2082−2084.
(44) De Trizio, L.; Prato, M.; Genovese, A.; Casu, A.; Povia, M.; Simonutti, R.; Alcocer, M. J. P.; D'Andrea, C.; Tassone, F.; Manna, L. Strongly Fluorescent Quaternary Cu-In-Zn-S Nanocrystals Prepared from $Cu_{1-x}InS_2$ Nanocrystals by Partial Cation Exchange. *Chem. Mater.* **2012**, *24*, 2400−2406.
(45) Kolny-Olesiak, J.; Weller, H. Synthesis and Application of Colloidal $CuInS_2$ Semiconductor Nanocrystals. *ACS Appl. Mater. Interfaces* **2013**, *5*, 12221−12237.
(46) Li, L.; Pandey, A.; Werder, D. J.; Khanal, B. P.; Pietryga, J. M.; Klimov, V. I. Efficient Synthesis of Highly Luminescent Copper Indium Sulfide-Based Core/Shell Nanocrystals with Surprisingly. *J. Am. Chem. Soc.* **2011**, *133*, 1176−1179.
(47) Kim, Y. K.; Ahn, S. H.; Chung, K.; Cho, Y. S.; Choi, C. J. The Photoluminescence of $CuInS_2$ Nanocrystals: Effect of Non-Stoichiometry and Surface Modification. *J. Mater. Chem.* **2012**, *22*, 1516−1520.
(48) Tang, X.; Yu, K.; Xu, Q.; Choo, E. S. G.; Goh, G. K. L.; Xue, J. Synthesis and Characterization of $AgInS_2$−ZnS Heterodimers with Tunable Photoluminescence. *J. Mater. Chem.* **2011**, *21*, 11239−11243.
(49) Tang, X.; Cheng, W.; Choo, E. S. G.; Xue, J. Synthesis of $CuInS_2$−ZnS alloyed Nanocubes with High Luminescence. *Chem. Commun.* **2011**, *47*, 5217−5219.
(50) Zhang, W.; Zhong, X. Facile Synthesis of ZnS−$CuInS_2$-Alloyed Nanocrystals for a Color-Tunable Fluorchrome and Photocatalyst Long-Lived Emission. *Inorg. Chem.* **2011**, *50*, 4065−4072.
(51) Jun, Y.; Lee, S. M.; Kang, N. J.; Cheon, J. Controlled Synthesis of Multi-armed CdS Nanorod Architectures Using Mono surfactant System. *J. Am. Chem. Soc.* **2001**, *123*, 5150−5151.
(52) Ogawa, T.; Kuzuya, T.; Hamanaka, Y.; Sumiyama, S. Synthesis of Ag−In Binary Sulfide Nanoparticles—Structural Tuning and Their Photoluminescence Properties. *J. Mater. Chem.* **2010**, *20*, 2226−2231.
(53) Nose, K.; Fujita, N.; Omata, T.; Otsuka-Yao-Matsuo, S.; Kato, W.; Uehara, M.; Nakamura, H.; Maeda, H.; Kamioka, H.; Hosono, H. Photoluminescence of $CuInS_2$-based Semiconductor Quantum Dots; Its Origin and The Effect of ZnS Coating. *J. Phys. (Paris)* **2009**, *165*, 012028.
(54) Oh, J. H.; Yang, S. J.; Do, Y. R. Healthy, Natural, Efficient and Tunable Lighting: Four-Package White LEDs for Optimizing The Circadian Effect, Color Quality, and Vision Performance. *Light Sci. Appl.* **2014**, *3*, e141.
(55) Ohno, Y. Spectral Design Considerations for White LED Color Rendering. *Opt. Eng.* **2005**, *44*, 111302.
(56) Ohno, Y. Color Rendering and Luminous Efficacy of White LED Spectra. *Proc. SPIE* **2004**, *5530*, 88−98.


DOI: 10.1021/acsami.5b00664
*ACS Appl. Mater. Interfaces* 2015, 7, 7342−7350